JACS
JOURNAL OF THE AMERICAN CHEMICAL SOCIETY

ARTICLE

pubs.acs.org/JACS

Role of Coordination Geometry in Dictating the Barrier to Hydride Migration in d^6 Square-Pyramidal Iridium and Rhodium Pincer Complexes

Michael Findlater, Alison Cartwright-Sykes, Peter S. White, Cynthia K. Schauer,* and Maurice Brookhart*

Department of Chemistry, The University of North Carolina at Chapel Hill, Chapel Hill, North Carolina 27599-3290, United States

Supporting Information

ABSTRACT: Syntheses of the olefin hydride complexes [(POCOP)M(H)(olefin)][BAr^f_4] (**6a-M,** M = Ir or Rh, olefin = C_2H_4; **6b-M**, M = Ir or Rh, olefin = C_3H_6; POCOP = 2,6-bis-(di-*tert*-butylphosphinito)benzene; BAr^f = tetrakis(3,5-trifluoromethylphenyl)borate) are reported. A single-crystal X-ray structure determination of **6b-Ir** shows a square-pyramidal coordination geometry for Ir, with the hydride ligand occupying the apical position. Dynamic NMR techniques were used to characterize these complexes. The rates of site exchange between the hydride and the olefinic hydrogens yielded $\Delta G^{\ddagger}$ = 15.6 (**6a-Ir**), 16.8 (**6b-Ir**), 12.0 (**6a-Rh**), and 13.7 (**6b-Rh**) kcal/mol. The NMR exchange data also established that hydride migration in the propylene complexes yields exclusively the primary alkyl intermediate arising from 1,2-insertion. Unexpectedly, no averaging of the top and bottom faces of the square-pyramidal complexes is observed in the NMR spectra at high temperatures, indicating that the barrier for facial equilibration is >20 kcal/mol for both the Ir and Rh complexes. A DFT computational study was used to characterize the free energy surface for the hydride migration reactions. The classical terminal hydride complexes, [M(POCOP)(olefin)H]$^+$, are calculated to be the global minima for both Rh and Ir, in accord with experimental results. In both the Rh ethylene and propylene complexes, the transition state for hydride migration (TS1) to form the agostic species is higher on the energy surface than the transition state for in-place rotation of the coordinated C−H bond (TS2), while for Ir, TS2 is the high point on the energy surface. Therefore, only for the case of the Rh complexes is the NMR exchange rate a direct measure of the hydride migration barrier. The trends in the experimental barriers as a function of M and olefin are in good agreement with the trends in the calculated exchange barriers. The calculated barriers for the hydride migration reaction in the Rh complexes are ∼2 kcal/mol higher than for the Ir complexes, despite the fact that the energy difference between the olefin hydride ground state and the agostic alkyl structure is ∼4 kcal/mol larger for Ir than for Rh. This feature, together with the high barrier for interchange of the top and bottom faces of the complexes, is proposed to arise from the unique coordination geometry of the agostic complexes and the strong preference for a *cis*-divacant octahedral geometry in four-coordinate intermediates.

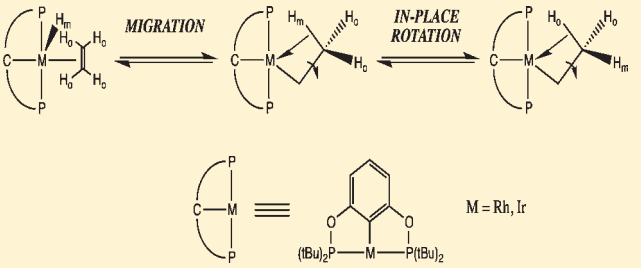

INTRODUCTION

Migratory insertion reactions of transition metal olefin hydride and olefin alkyl complexes are key transformations in a variety of catalytic reactions, including olefin hydrogenation, hydroformylation, isomerization, polymerization, and oligomerization.[1] The classical view of the migratory insertion reaction of a metal olefin hydride complex is illustrated in Scheme 1 with ethylene hydride complex, **1**, and involves the transformation of this species to a high energy unsaturated ethyl intermediate, **3**, via a transition state, **2**, in which hydrogen is bridged between the metal and the β-carbon. The barriers to such migratory insertion processes have often been examined by measuring the rates of hydrogen scrambling between the metal hydride and olefinic sites through either dynamic NMR studies or, on slower time scales, through H/D scrambling reactions.[2]

While this is an appealingly simple picture, the actual situation is often much more complex (Scheme 2). The most stable form

Scheme 1. Classical Picture of Migratory Insertion in an Ethylene Hydride Complex

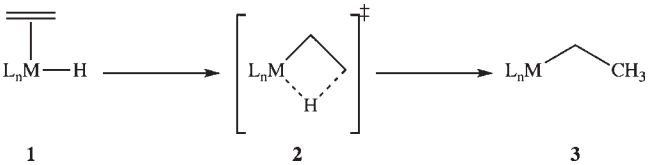

1 **2** **3**

of numerous "olefin hydride" complexes (particularly late metal, first-row, electrophilic species) often proves to be the bridged, agostic species, **2′**.[3−6] There is growing evidence that the scrambling between the agostic hydrogen and the terminal

Received: May 26, 2011
Published: June 24, 2011

hydrogens in such species occurs by an "in-place" rotation around C_α-C_β and not by formation of a true unsaturated metal alkyl complex, which exhibits no β-CH−metal contact.[7] Similarly, hydrogen exchange in classical olefin hydride complexes likely occurs via formation of an agostic intermediate followed by in-place rotation. The unsaturated metal alkyl complexes in these cases represent high-energy species and may not be true intermediates. Experimental studies are often insufficient to distinguish the classical description (Scheme 1) from the mechanism in Scheme 2, and computational studies have been invaluable in refining the subtle features of these processes.[8]

This situation is clearly illustrated by the structure and dynamics of the cationic Co(III) ethylene hydrides and their Rh(III) congeners shown in Scheme 3.[9−11] These d^6, 18-electron complexes possess geometries which are best described as distorted octahedral. The stable form of the cobalt complexes, **4**, is the agostic structure as shown.[8,9] The barriers to scrambling of the agostic H with the terminal hydrogens lie in the range 9.2−13.4 kcal/mol, and the scrambling process was presumed to proceed via the 16-electron ethyl complex, **4′**. Computational studies indicate such scrambling occurs by in-place rotation and that the 16-electron species, **4′**, is energetically inaccessible. The α-agostic species **4″** is calculated to be more stable than the unsaturated ethyl complex **4′**.[7]

A similar situation holds for the Rh complexes, **5**.[10] The global minimum is the olefin hydride species, **5**, and measured scrambling barriers are considerably higher (12−15 kcal/mol) than those for the cobalt analogues. Computations show that the scrambling occurs via the formation of the agostic species, **5′**, followed by in-place rotation. The Rh 16-electron ethyl complex is calculated to be very high in energy and less stable than the α-agostic isomer.[7a]

Similarly, experimental[12] and theoretical[13] studies of d^8, 16-electron, square-planar complexes of the type $[(\text{diimine})M-R]^+$ (M = Ni, Pd, Pt; R = C_nH_{2n+1}, $n > 1$) have shown that β-agostic structures are adopted for M = Ni or Pd, while Pt exhibits a classical olefin hydride structure. The barriers to scrambling of the agostic H with the terminal hydrogens increase upon descending the group; for example, a free energy of activation of 19.2 kcal/mol (337 K) was determined for hydride migration in the ethylene hydride complex $[[2,6\text{-}Me_2C_6H_3)N{=}C(An)-C(An){=}N(2,6\text{-}Me_2C_6H_3)]Pt(H)-(\text{ethylene})[BAr^f_4]$.[12a] Similarly, the barriers for methyl migration in related cationic M(II) alkyl ethylene complexes fall in the range of 13−14 kcal/mol for Ni(II), 17−19 kcal/mol for Pd(II), and 30 kcal/mol for Pt(II).[12]

We report here an investigation of the synthesis and migratory insertion of pincer-supported square-pyramidal d^6, 16-electron Ir(III) and Rh(III) olefin hydride complexes. By virtue of the rigid meridionally coordinated pincer ligand, we are able to experimentally determine that the barrier for scrambling of the metal hydride with the hydrogens of the ethylene ligands via an

Scheme 2. Hydrogen Scrambling Processes in Ethylene Hydride Complex, 1, and the β-Ethyl Agostic Complex, 2′

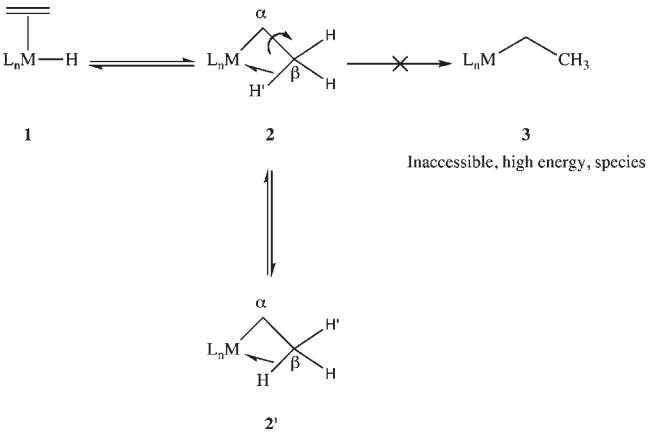

Scheme 3

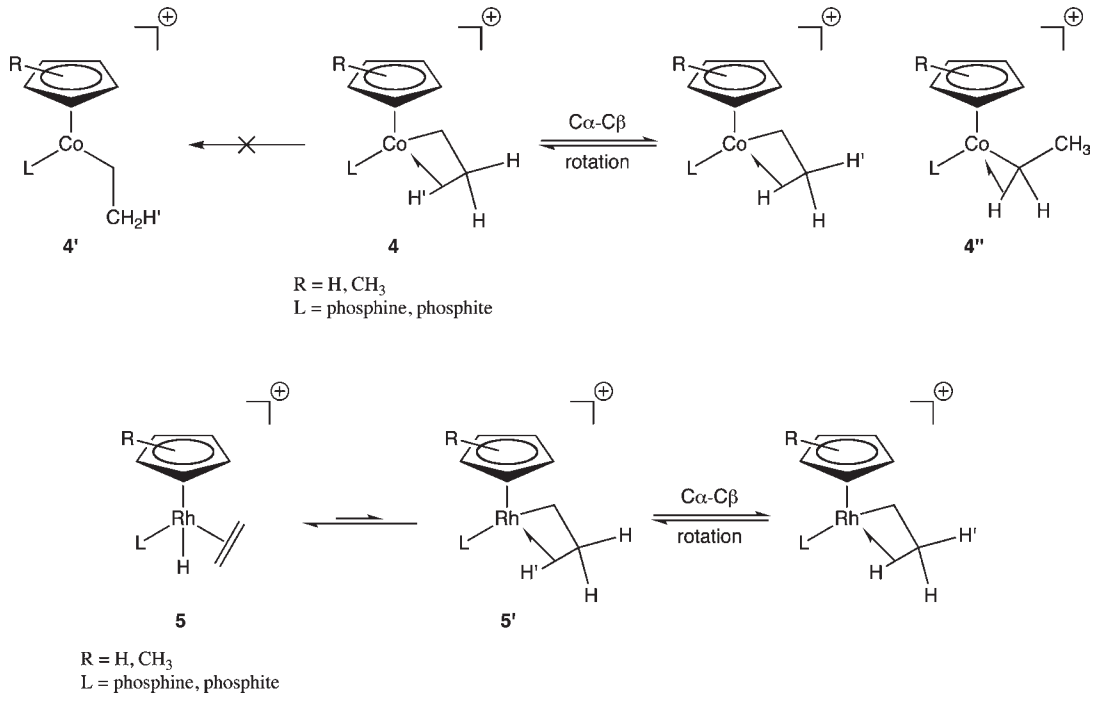

dx.doi.org/10.1021/ja204851x |J. Am. Chem. Soc. 2011, 133, 12274–12284

in-place rotation mechanism is lower than the barrier for formation of a square-planar 14-electron ethyl complex by at least 9 kcal/mol for Rh and 5.5 kcal/mol for Ir. Experimental studies are augmented by DFT calculations. In addition, dynamics of the analogous propylene complexes are reported which show that scrambling occurs preferentially via a 1,2-insertion mechanism.

■ RESULTS AND DISCUSSION: SYNTHESIS AND DYNAMICS OF OLEFIN HYDRIDE COMPLEXES

Synthesis and Characterization of [(POCOP)M(H)(L)][BAr$^f_4$] (M = Ir, L = C_2H_4 (6a-Ir); M = Rh, L = C_2H_4 (6a-Rh); M = Ir, L = C_3H_6 (6b-Ir); and M = Rh, L = C_3H_6 (6b-Rh)). Olefin hydride complexes can be cleanly generated by purging a mixture of (POCOP)M(H)(Cl)[14] and NaBAr$^f_4$ in methylene chloride solvent with either ethylene or propylene gas (Scheme 4). Reactions are complete within 15 min, as indicated by a color change from light red to pale orange. Removal of sodium chloride by syringe filtration under argon and evaporation of the solvent yields pure products as pale orange powders. However, the propylene complex **6b-Rh** is unstable at room temperature in methylene chloride in the absence of an excess of propylene.[14b]

Scheme 4. Preparation of Complexes 6a-Ir, 6a-Rh, 6b-Ir, and 6b-Rh

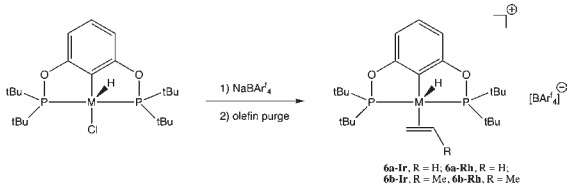

At room temperature the bound ethylene of **6a-Ir** is rapidly rotating on an NMR time scale, as is evident by a single ethylene resonance in the ^{1}H NMR spectrum at 4.15 ppm in CD_2Cl_2. The upfield shift of the iridium hydride at −42.8 ppm in **6a-Ir** is consistent with a five-coordinate complex in which the hydride is situated in the apical position *trans* to an empty coordination site. In marked contrast, the ^{1}H NMR spectrum of **6a-Rh** under ambient conditions displays neither ethylene nor hydride signals, which suggests that exchange between these sites via migratory insertion is occurring on a time scale that broadens these signals into the baseline. Indeed, upon cooling a CD_2Cl_2 solution of **6a-Rh** to temperatures below ca. 283 K in the NMR probe, a single broad resonance is observed at 4.59 ppm, corresponding to the bound ethylene, with concomitant appearance of the Rh−hydride resonance at −28.61 ppm as a doublet of triplets ($^1J_{Rh-H}$ = 51.0 Hz, $^2J_{P-H}$ = 9.0 Hz).

Both ethylene complexes have a geometry that requires the *tert*-butyl groups *syn* to the hydride to be distinct from those *anti* to the hydride. Indeed, two *tert*-butyl signals (seen as virtual triplets due to strong phosphorus−phosphorus coupling) are observed in the ^{1}H NMR spectra for both **6a-Ir** and **6a-Rh**, suggesting the existence of a vertical mirror plane bisecting the ligand backbone. This analysis is supported by a single ^{31}P resonance at 182.0 ppm for the two equivalent phosphorus atoms in **6a-Ir** and a doublet centered at 205.3 ppm ($^1J_{Rh-P}$ = 105 Hz) for **6a-Rh.**

The propylene complexes **6b-Ir** and **6b-Rh** display some characteristics similar to the ethylene complexes; however, there

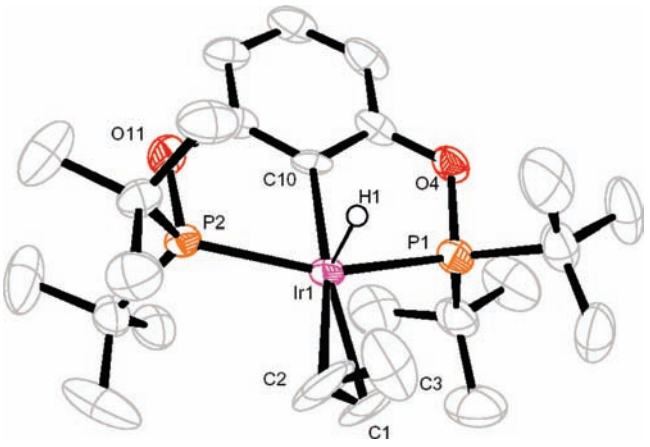

Figure 1. ORTEP diagram of [(POCOP)Ir(H)(C_3H_6)][BAr^f] (**6b-Ir**). The hydrogen atoms and counterion have been excluded for clarity. Thermal ellipsoids shown at 40% probability. Key bond distances and bond angles: Ir(1)−C(10) 2.046 Å, Ir(1)−P(1) 2.338 Å, Ir(1)−P(2) 2.338 Å, Ir(1)−C(1) 2.255 Å, Ir(1)−C(2) 2.276 Å, C(1)−C(2) 1.141 Å, P(1)−Ir(1)−C(10) 78.57°, P(2)−Ir(1)−C(10) 78.72°, C(2)−C(1)−Ir(1)−P(2) −39.78°. Errors in metrical parameters are omitted due to disorder in the structure.

are some notable differences. In **6b-Ir**, the iridium hydride resonance appears as a broadened triplet at −42.90 ppm, analogous to ethylene complex **6a-Ir**. The aryl backbone of the ligand in **6a-Ir** has two resonances associated with it, a triplet for H_4 (*para* to the iridium-bound carbon) and a doublet for the two equivalent hydrogens (H_3 and H_5) adjacent to H_4. In the propylene complex **6b-Ir**, H_3 and H_5 are now inequivalent and appear as two doublets in the ^{1}H NMR spectrum at 6.90 and 6.86 ppm. There are also now four resonances for the *tert*-butyl groups, indicating that none of the *tert*-butyl groups are symmetry equivalent. Consistent with these observations, the ^{31}P NMR spectrum exhibits two doublets (182.7 ppm, 175.0 ppm, J_{P-P} = 260 Hz). It is likely that the propylene ligand, similar to the ethylene ligand, is also rotating rapidly at room temperature (see below); however, since none of the conformations possess a mirror plane bisecting the ligand backbone, rapid rotation does not result in averaging the ^{31}P signals, H_3 with H_5, or any of the *tert*-butyl resonances.

The molecular structure of [(POCOP)Ir(H)(C_3H_6)][BAr$^f_4$] (**6b-Ir**) was established via single-crystal X-ray diffraction. A crystal suitable for X-ray analysis was grown by slow diffusion of pentane into a methylene chloride solution of **6b-Ir** at room temperature under an argon atmosphere. An ORTEP diagram of **6b-Ir** is shown in Figure 1. The propylene ligand is rotated from alignment of the C−C double bond with the plane of the ligand backbone. This rotation likely occurs to decrease the steric interactions between the methyl group of the propylene ligand and the *tert*-butyl substituents on phosphorus. A slight disordering in the propylene ligand prevents a meaningful discussion of the bond lengths of the ligated olefin in this structure.

Kinetics of Migratory Insertion Processes. The rate of site exchange between the hydride and ethylene hydrogens of **6a-Ir** was determined using line-broadening techniques. As the temperature is raised to 320 K (C_6D_5Cl solution), both the ethylene and hydride resonances broaden (Figure 2). To verify that the observed broadening was due to insertion, a spin-saturation transfer experiment was performed. At 276 K, when the hydride signal was irradiated, the ethylene signal decreased 49%, clearly

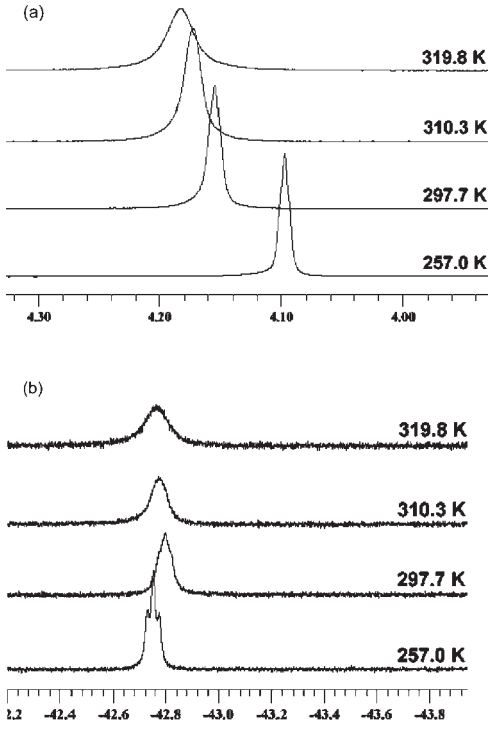

Figure 2. High-temperature ^{1}H NMR stacked plots of the ethylene (a) and hydride (b) resonance of [(POCOP)Ir(H)(C_2H_4)][BAr^f_4] (**6a-Ir**).

showing that the observed line broadening of the hydride and ethylene signals is due to exchange through a migratory insertion process.

Since the population ratios are 4:1, the hydride resonance broadens at 4 times the rate of the ethylene signal. Applying the slow exchange approximation ($k = \pi\Delta W$) to line widths at half-heights for these signals yields a rate for exchange of Ir−H into the ethylene ligand of 58 s^{-1} at 310 K and 148 s^{-1} at 320 K, corresponding to $\Delta G^{\ddagger}$ = 15.6 kcal/mol. Similar values are obtained from analysis of the broadening of the ethylene signal when a statistical correction is applied.[15]

Notably, the two resonances for the *tert*-butyl signals do not average in a similar fashion. The *tert*-butyl resonances remain sharp up to temperatures as high as 383 K (line width change less than 3 Hz, conservatively), indicating a rate of averaging of less than 10 s^{-1} and a barrier to averaging the "top" and "bottom" faces of the complex of greater than ca. 21 kcal/mol. In other words, there is a high barrier for formation of a symmetrical 14-electron ethyl complex, which can collapse to either face of the pincer ligand and re-form the stable ethylene hydride. This is addressed in more detail below when describing the DFT results.

The behavior of the rhodium ethylene hydride complex **6a-Rh** is similar to that of **6a-Ir** except that the barrier to scrambling is lower. Using the same analysis of line broadening of the hydride resonance as for **6a-Ir**, the rate constant for exchange of the Rh−H with the ethylene hydrogens is 9.0 s^{-1} at 229 K and 276 s^{-1} at 253 K, corresponding to $\Delta G^{\ddagger}$ = 12.0 kcal/mol. As for **6a-Ir**, the *tert*-butyl resonances remain sharp up to 373 K, indicating a barrier greater than 20.5 kcal/mol for face-to-face switching of the ethyl group.[15]

Low-temperature NMR analysis of the iridium and rhodium ethylene complexes, **6a-Ir** and **6a-Rh**, provided no information concerning the barrier to ethylene rotation. However, NMR analysis of the propylene complexes, **6b-Ir** and **6b-Rh**, does yield information concerning the rotational barrier in these more hindered systems. The variable-temperature NMR spectra in CD_2Cl_2 of **6b-Ir** are shown in Figure 3. The propylene vinylic and methyl signals as well as the Ir−H resonance all broaden below ca. 223 K, and at 175 K there is clear evidence for a set of signals for both a minor isomer and a major isomer. Signals marked **1a**−**4a** correspond to the major isomer, while signals marked **1b**−**4b** correspond to the minor isomer, with the isomer ratio equal to ca. 0.066 at 175 K. Both hydride resonances at −42.56 (minor) and −43.20 (major) ppm indicate that both isomers are five-coordinate species with a vacant coordination site trans to the hydride ligand, ruling out a minor species involving solvent coordination. The observation of two distinct hydride resonances in a ratio of 0.056 at −26.72 (minor) and −28.38 (major) ppm in the ^{1}H NMR spectrum of **6b-Rh** at 193 K suggests a similar situation for the rhodium complex.

Structures of the two possible rotamers of **6b-Ir** are shown in Scheme 5; the *syn* rotamer is the isomer that was crystallographically characterized. Using line-broadening techniques together with the experimentally determined K_{eq} value, the rate constant for conversion of the minor rotamer to the major rotamer, $k_{min\text{-}to\text{-}maj}$, was determined to be 16 s^{-1} (205 K, $\Delta G^{\ddagger}$ = 9.1 kcal/mol), with $k_{maj\text{-}to\text{-}min}$ = 1.2 s^{-1} ($\Delta G^{\ddagger}$ = 10.2 kcal/mol).

For the **6b-Ir**, insertion of propylene into the M−H bond could lead to two possible agostic intermediates, a linear species (from 1,2-insertion) and a branched species (from 2,1 insertion), as shown in Scheme 6. Spin-saturation-transfer NMR experiments (Figure 4, 296 K) were used to determine the favored mode of insertion. Spectrum E shows the 1-H vinyl region as well as the hydride region of the spectrum, with peak assignments given at the top of the figure. Site exchange between a pair of resonances is indicated by a decrease in intensity of the companion signal upon saturation of an individual resonance. Spectrum A of Figure 4 shows that when the resonance for H_c is irradiated, only the signal for H_b decreases in intensity. Complementary results are seen in spectrum B, showing that irradiation of H_b only reduces the intensity of the H_c signal. Spectrum C shows that irradiation of H_a only decreases the hydride signal intensity, H_d, and conversely in spectrum D, irradiation of H_d only decreases H_a. The pairwise exchange of H_b/H_c and H_a/H_d supports the proposal that the insertion of propylene into the Ir−H bond preferentially forms the linear (1,2-insertion) product.

As mentioned above, the propylene complex has both "top/bottom" and "side-to-side" inequivalence. Insertion of propylene into the Ir−H bond results in a species with an average mirror plane bisecting and perpendicular to the ligand plane, as observed in the variable-temperature ^{1}H NMR spectra. The H_3 and H_5 hydrogens of the ligand backbone merge into one doublet from two, and the two pairs of *tert*-butyl resonances broaden and merge into two triplets. Even at elevated temperatures, the "top" and "bottom" faces do not equilibrate, consistent with observations for the ethylene complexes **6a-Ir** and **6a-Rh**. Spin-saturation-transfer NMR techniques were used to measure the rate of insertion of propylene into the M−H bond in **6b-Ir** and **6b-Rh**. Using the spin−lattice relaxation time in combination with the extent of signal reduction upon irradiation, standard equations can be applied to determine exchange rates (see Supporting Information for details). Using data from irradiation of H_a at 6.50 ppm, the rate of exchange via migratory insertion was estimated to be 2.6 s^{-1} at 296 K, corresponding to a free energy

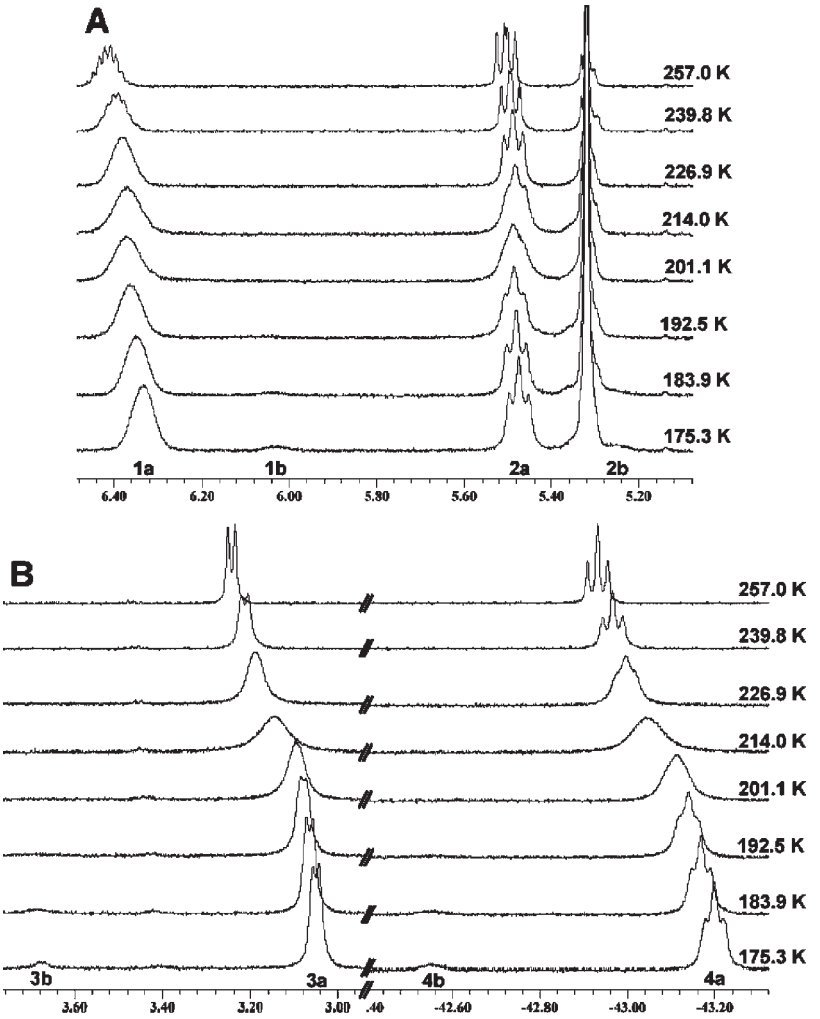

Figure 3. Variable-temperature stacked ^{1}H NMR spectra of [(POCOP)Ir(H)(C_3H_6)][BAr^f_4] (**6b-Ir**).

Scheme 5. Two Possible Rotamers of [(POCOP)Ir(H)(C_3H_6)][BAr^f_4] (6b-Ir)

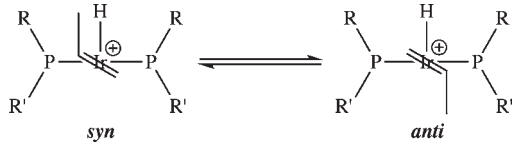

barrier of 16.8 kcal/mol. This value is similar to the value of 15.6 kcal/mol determined for migratory insertion in **6a-Ir**. Similar analysis of the dynamic behavior of the rhodium analogue, **6b-Rh**, via irradiation of the H_c signal at 3.64 ppm yields a rate of exchange estimated to be 4.9 s^{-1} at 247 K, corresponding to a free energy barrier of 13.7 kcal/mol.

Computational Studies. To gain additional insight into the experimentally observed rate of exchange between the hydride and alkene ligands in the [(POCOP)M(H)($CH_2C(H)(R)$]$^+$ pincer complexes, a computational study was undertaken. In addition to obtaining structural and energetic information on the unobserved alkyl agostic species relative to the alkene hydride ground state, an additional feature that the computational studies address is the large barrier for exchanging the top and bottom faces of the complex via the alkyl agostic intermediate.

A description of the computational methodology is given in the Experimental Section. The optimized singlet ground- and transition-state structures for the iridium ethylene and propylene analogues are shown in parts a and b, respectively, of Figure 5, and selected bond distances and angles for both the rhodium and iridium analogues are reported in Table 1. The lowest energy triplets lie >28 kcal/mol higher in energy, suggesting that the hydride migration reactions take place on the singlet surface.

The structures of the [(POCOP)M(H)($CH_2C(H)(R)$]$^+$ complexes are based on a square-pyramidal geometry in which the hydride ligand sits in the apical position and the alkene ligand is positioned *trans* to the aryl carbon of the pincer ligand (C_p) (Figure 5). The alkene is rotated by 42° (Ir) and 29° (Rh) with respect to the plane of the pincer ligand. In computations on a trimmed complex in which the *tert*-butyl groups were replaced by Me groups, the alkene carbon atoms lie in the plane of the pincer ligand for the lowest energy conformer, indicating that steric requirements of the *tert*-butyl groups dictate the observed conformation of the alkene ligand. In the calculated structures of the [M(POCOP)(CH_2CH_2R)]$^+$ β-agostic complexes, **7a-M** (M = Rh or Ir, olefin = C_2H_4) and **7b-M** (M = Rh or Ir, olefin = C_2H_3Me)

dx.doi.org/10.1021/ja204851x |*J. Am. Chem. Soc.* 2011, 133, 12274–12284

Scheme 6. The Two Possible Modes of Propylene Insertion into the M−H Bond in 6b-Ir and 6b-Rh

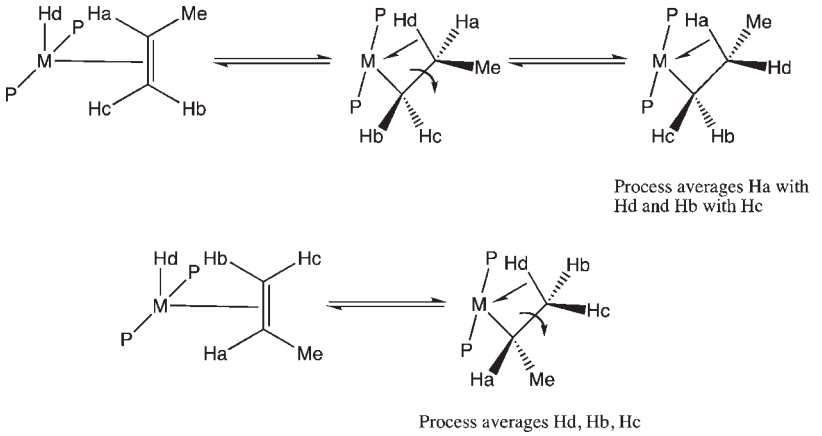

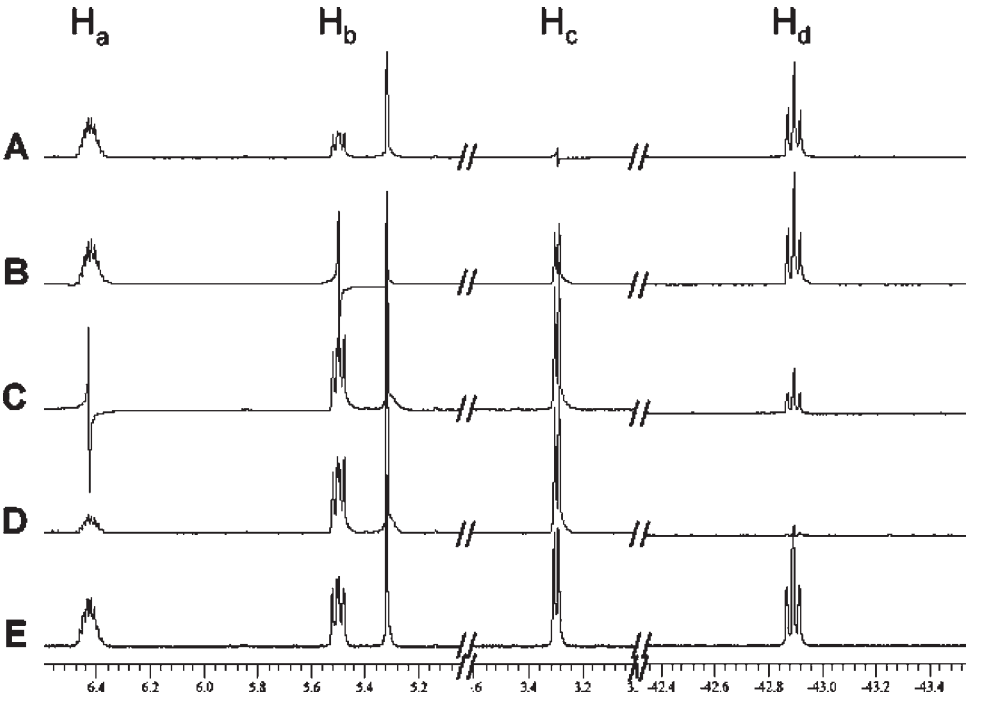

Figure 4. Spin-saturation-transfer experiment for **6b-Ir**.

(Figure 5), the coordinated C−H bond is positioned *trans* to the pincer carbon (C_p). The appended alkyl carbon atom is centered in the cleft between the two *tert*-butyl groups and distorted away from the apical position in an ideal square pyramid (C_p−M−C_α = 123−129°).

The energy profiles for the hydride migration and in-place rotation reactions are shown in Figure 6, and the calculated energies are summarized in Table 2. In accord with experiment, the olefin hydride complexes, **6**, are calculated to be the ground states for both the Rh and Ir systems. The agostic species, **7**, lie 6 kcal/mol (Ir) and 2 kcal/mol (Rh) higher in energy for the ethylene complexes and 7 kcal/mol (Ir) and 5 kcal/mol (Rh) higher in energy for the propylene complexes. Despite the larger energy differences between the olefin hydride and alkyl agostic species for Ir, the calculated barriers for hydride migration to form the agostic species are higher for Rh than Ir for both the ethylene (8 kcal/mol (Ir) and 10 kcal/mol (Rh)) and propylene (10 kcal/mol (Ir) and 12 kcal/mol (Rh)) systems. The hydrogen atom in the transition state for hydride migration approaches the fourth coordination site *trans* to the pincer arene ligand (see Figure 5), leaving the axial sites effectively vacant like in a square-planar geometry. The higher calculated hydride migration barrier for Rh may be related to the higher barrier for passing through a square-planar geometry calculated for Rh in comparison to Ir in model $[M(POCOP\text{-}Me)H]^+$ complexes (see discussion below).

The experimentally observed NMR exchange between the hydride resonance and the olefin C−H resonance requires hydride migration together with interchange of the coordinated C−H bonds via an in-place rotation.[6] Based on the calculated energy profiles (Figure 6), the experimental barrier for the Rh systems is a direct measure of the barrier for hydride migration, while for Ir, the experimental barrier is the sum of the ground-state energy

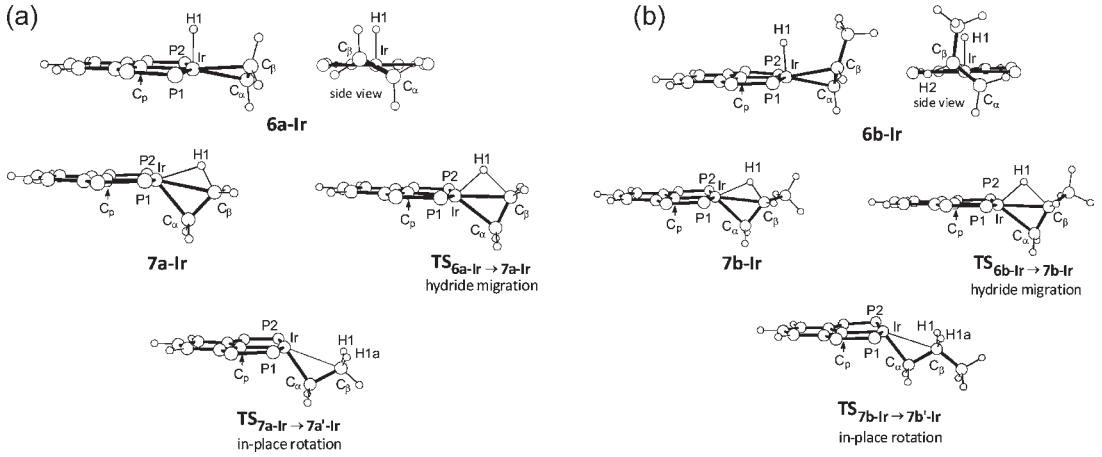

Figure 5. Optimized ground- and transition-state structures for (a) the $[(POCOP)Ir(ethylene)(H)]^+$ system and (b) the $[(POCOP)Ir(propylene)(H)]^+$ system.

Table 1. Bond Distances (Å) and Angles (°) for Calculated Structures

compound	M−P1	M−P2	M−C_p	M−C_α	M−C_β	M−H1	C_α−C_β	C_β−H1[a]	C_p−M−C_α (H)[b]	C_p−M−C_β	M−C_α−C_β
6a-Ir	2.35	2.35	2.04	2.23	2.25	1.52	1.39		89		
7a-Ir	2.36	2.36	1.98	2.04	2.37	1.88	1.49	1.18	129	168	83
$TS_{6a\text{-}Ir\rightarrow 7a\text{-}Ir}$	2.35	2.35	2.00	2.15	2.28	1.60	1.42	1.56	145	178	77
$TS_{7a\text{-}Ir\rightarrow 7a'\text{-}Ir}$	2.37	2.37	1.96	2.02	2.64	2.81	1.53	1.10	124	159	95
6b-Ir	2.36	2.35	2.03	2.24	2.32	1.52	1.39		87		
7b-Ir	2.36	2.36	1.98	2.06	2.39	1.85	1.49	1.19	134	171	83
$TS_{6b\text{-}Ir\rightarrow 7b\text{-}Ir}$	2.35	2.36	2.01	2.15	2.32	1.60	1.42	1.60	144	175	79
$TS_{7b\text{-}Ir\rightarrow 7b'\text{-}Ir}$	2.36	2.35	1.96	2.03	2.68	2.80	1.53	1.10	125	160	97
6a-Rh	2.34	2.34	2.02	2.27	2.28	1.49	1.38		85		
7b-Rh	2.37	2.37	1.97	2.01	2.37	1.93	1.50	1.15	123	162	84
$TS_{6a\text{-}Rh\rightarrow 7a\text{-}Rh}$	2.36	2.36	2.00	2.17	2.27	1.55	1.40	1.59	151	172	75
$TS_{7a\text{-}Rh\rightarrow 7a'\text{-}Rh}$	2.38	2.37	1.95	2.00	2.60	2.78	1.52	1.10	117	153	95
6b-Rh	2.35	2.34	2.01	2.28	2.38	1.49	1.37		83		
7b-Rh	2.38	2.38	1.98	2.02	2.38	1.92	1.50	1.16	126	164	84
$TS_{6b\text{-}Rh\rightarrow 7b\text{-}Rh}$	2.36	2.37	2.01	2.16	2.32	1.55	1.40	1.64	148	173	78
$TS_{7b\text{-}Rh\rightarrow 7b'\text{-}Rh}$	2.37	2.36	1.95	2.01	2.64	2.75	1.52	1.10	120	155	96

[a] A typical calculated C−H bonding distance is 1.09 Å. [b] C_p−M−H angle for the alkene complexes.

difference between the olefin hydride and agostic species ($\Delta E_{\mathbf{6\text{-}Ir}\rightarrow\mathbf{7\text{-}Ir}}$) and the barrier for in-place rotation. The calculated barriers are in reasonable agreement with the experimental barriers (see Table 2), and the trends (as functions of metal and olefin) in the experimental data are reproduced.

The transition state for in-place rotation for agostic **7a** is pictured in Figure 5a ($TS_{\mathbf{7a\text{-}Ir}\rightarrow\mathbf{7a'\text{-}Ir}}$). The interaction between the coordinated methyl group and Ir is considerably diminished in the transition state, as signified by an increase in the Ir−C_β distance from 2.37 to 2.64 Å and an opening up of the Ir−C_α−C_β angle from 83° to 95°. To obtain an estimate of the strength of the agostic interaction, a potential energy scan was carried out for a trimmed version of **7a-Ir**, in which the t-Bu groups were replaced by Me groups. The C_p−Ir−C_α angle was stepped from 90° to the 128° value for the minimum energy structure with a geometry optimization at each step. The structure with a C_p−Ir−C_α = 90° and Ir−C_α−C_β = 107°, in which the ethyl ligand adopts a staggered configuration, lies ca. 10 kcal/mol to higher energy than the minimum with C_p−Ir−C_α = 128°. This net 10 kcal/mol energy difference includes a 3 kcal/mol stabilization arising from adoption of a staggered configuration by the ethyl ligand. A similar analysis for the rhodium system yields a 5 kcal/mol energy difference for the structure with a C_p−Rh−C_α angle of 90° and a Rh−C_α−C_β angle of 104°.

The DFT calculations also agree well with the experimental results in the propylene system. NMR evidence was obtained for two rotamers of the propylene ligands in **6b-Ir**. The crystallographically characterized rotamer corresponds to the lowest energy rotamer determined computationally, which is pictured in Figure 5. The energy difference between the two rotamers of ~1 kcal/mol is in reasonable agreement with the experimental rotamer ratio (15:1 at 175 K). The calculated barrier for propylene rotation in **6b-Ir** is 10 kcal/mol, which agrees well with the experimental value of 10 kcal/mol obtained from line-broadening measurements. Hydride migration to the major

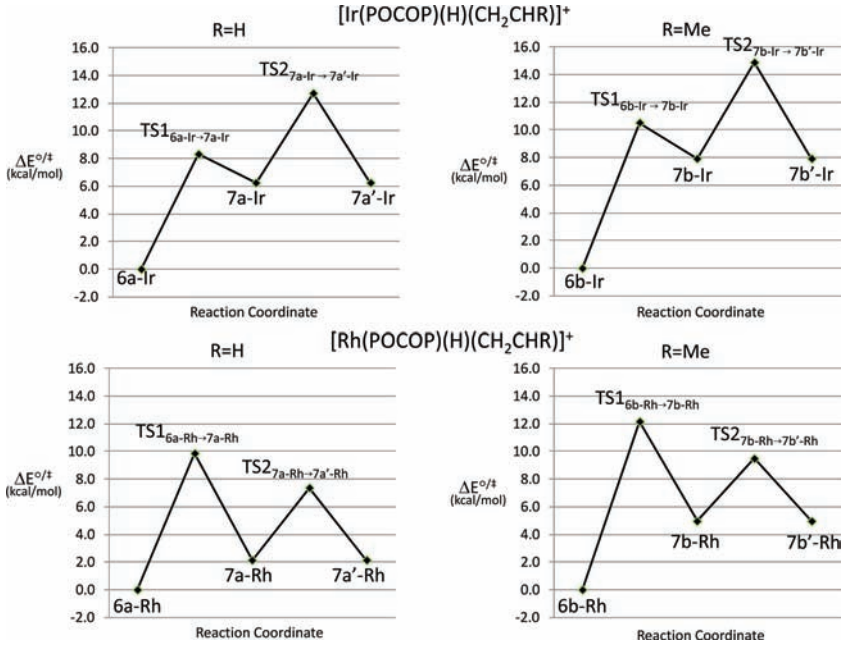

Figure 6. Energy profile for the $[(POCOP)M(H)(olefin)]^+$ system.

Table 2. Calculated Ground-State and Transition-State Energies (kcal/mol)

M	olefin	ML(olefin)(H)$^+$	ML(agostic)$^+$	TS1[a]	TS2[b]	exchange barrier[c]	expt $\Delta G^{\ddagger}$
Ir	C_2H_4	0.0	6.2	8.3	6.5	12.7	15.6
Rh	C_2H_4	0.0	2.1	9.8	5.1	9.8	12.0
Ir	C_2H_3Me	0.0	7.9	10.5	6.9	14.8	16.8
Rh	C_2H_3Me	0.0	5.0	12.2	4.5	12.2	13.7

[a] Transition state for hydride migration. [b] Transition state for in-place rotation. [c] For Ir, exchange barrier = ΔE(ML(agostic)$^+$ − ML(olefin)(H)$^+$) + TS2. For Rh, exchange barrier = TS1.

rotamer yields a primary alkyl agostic complex, while hydride migration to the minor rotamer yield a secondary alkyl agostic complex. The secondary alkyl agostic complex lies ~5 kcal/mol higher in energy than the primary agostic complex for both Rh and Ir, and the barrier for hydride migration to the minor rotamer (12 kcal/mol) is higher than the barrier for hydride migration to the major rotamer (10 kcal/mol). These computational results are consistent with the experimental result that only exchange resulting from hydride migration to the major rotamer is observed. Full details of calculations for the minor isomer are given in the Supporting Information.

A surprising feature in the NMR studies of the pincer alkene hydride complexes is that exchange of the top and bottom faces of the pincer complexes is not experimentally observed, and a lower limit to the barrier of ~20 kcal/mol is placed on both of these systems. The most reasonable pathway for interchanging the top and bottom faces of the pincer complex would involve decoordination of the agostic C−H bond to form a four-coordinate complex. The lowest energy structure for a four-coordinate d^6 pincer complex is based on a *cis*-divacant octahedron (eq 1),[16] with the alkyl group occupying one of the axial positions perpendicular to the plane of the POCOP ligand. Interchange of the top and bottom faces of these complexes would require the alkyl ligand to pass through a planar transition state to the opposite face of the complex, followed by rotation of the alkyl ligand about the M−C and C−C bonds to adopt the appropriate conformation for forming a new agostic interaction.

To explore the energetics of exchanging the top and bottom faces of the complex, calculations were carried out for a model hydride analogue, $[M(POCOP\text{-}Me)H]^+$ (**8-M**; M = Rh and Ir), with a trimmed ligand in which the t-Bu substituents are replaced by Me groups. The barrier for interchanging the hydride ligand between the two axial sites via a planar transition state (eq 1) on the singlet surface is 41 kcal/mol for **8-Ir** and 53 kcal/mol for **8-Rh**.

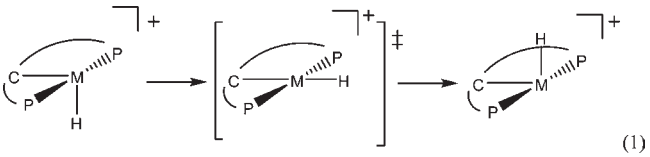

(1)

The barriers for equilibrating the two faces on the triplet surface are lower (7 kcal/mol for **8-Ir** and 6 kcal/mol for **8-Rh**), but the triplets lie considerably higher in energy than the singlet (28 kcal/mol for **8-Ir** and 31 kcal/mol for **8-Rh**). Given these large calculated barriers, it is not surprising that no exchange is observed between the top and bottom faces in the ethylene hydride complexes. For the d^6 configuration, conversion of the

dx.doi.org/10.1021/ja204851x |*J. Am. Chem. Soc.* 2011, 133, 12274–12284

C_s *cis*-divacant octahedral structure to the C_{2v} square-planar transition state is associated with a large reduction in the HOMO−LUMO gap and corresponding destabilization.

SUMMARY

Square-pyramidal cationic d^6 olefin hydride complexes of the type $[(POCOP)M(H)(olefin)][BAr^f_4]$ (**6a-M**, M = Ir or Rh, olefin = C_2H_4; **6b-M**, M = Ir or Rh, olefin = C_3H_6) have been synthesized and characterized by dynamic NMR spectroscopy. Rotation of the ethylene ligand is too fast to be measured by ^{1}H NMR spectroscopy. The ^{1}H spectra at −100 °C of propylene complexes **6b-Ir** and **6b-Rh** show two rotamers in a ca. 15:1 ratio. The barriers to interconversion of rotamers were determined using NMR techniques and are around 17 kcal/mol for **6b-Ir** and 14 kcal/mol for **6b-Rh**.

The rates of exchange between the hydride signal and the olefinic H signal were calculated for the ethylene and propylene complexes using line-broadening or spin-saturation transfer NMR techniques. The measured exchange barriers for the ethylene complexes are lower than for the propylene complex for both Rh and Ir ($\Delta G^{\ddagger}$ = 15.6 (**6a-Ir**), 12.0 (**6a-Rh**), 16.8 (**6b-Ir**), and 13.7 (**6b-Rh**) kcal/mol), and the barriers for the iridium complexes were higher than for the rhodium complexes for both pairs of complexes. No interchange between the top and bottom faces of the olefin hydride complexes is observed by NMR spectroscopy, setting a lower limit to the barrier of ∼20 kcal/mol.

Insight into the relationship between the NMR-measured exchange rates and the individual barriers to hydride migration (TS1) and in-place rotation (TS2) was obtained from a DFT study. The $[M(POCOP)(olefin)H]^+$ complexes are calculated to be the ground state for both Rh and Ir, in accord with experimental results, and the energy differences between the olefin hydride ground states and the alkyl agostic species are ∼2−4 kcal/mol larger for Ir than for Rh. For Rh, TS1 is the high point on the energy surface, while for Ir, TS2 is the high point; therefore, only for Rh is the experimental exchange barrier a measure of the hydride migration barrier. The square-pyramidal coordination geometry of the olefin hydrides, **6**, and the distorted square-pyramidal coordination for the alkyl agostic complexes, **7**, provide for some unusual trends in the barriers for these complexes. For a four-coordinate alkyl complex, which would be the intermediate preceding a face-to-face exchange of the alkyl ligand, a *cis*-divacant octahedron is the lowest energy structure. Computations on a model hydride complex indicate that the barriers for passing through a square-planar transition state to the opposite face on the singlet surface are sizable, and larger for Rh ($\Delta G^{\ddagger}$ = 51 kcal/mol) than for Ir ($\Delta G^{\ddagger}$ = 41 kcal/mol). Despite the larger ground-state energy difference calculated for Ir, the computed barriers to hydride migration are ∼2 kcal/mol higher for Rh than for Ir. This unusual feature may be related to the fact that the transition state for hydride migration samples this fourth site *trans* to the pincer arene ligand in a square-planar geometry, and therefore reflects the higher barrier for passing through this site calculated for Rh.

As noted earlier, the barriers to migratory insertion reactions of olefin hydride and olefin alkyl complexes in octahedral d^6 systems and in square-planar d^8 systems increase significantly moving from first-row to third-row homologues. This trend has important implications in catalysis; for example, catonic Ni(II) alkyl complexes are far more reactive in olefin oligomerization and polymerization reactions than analogous Pd(II) complexes, and Pd(II) complexes are more reactive than Pt(II) analogues. The present study suggests that this trend is reversed in d^6 five-coordinate, square-pyramidal Rh and Ir olefin hydride complexes. This observation could have significant implications for catalytic reactions involving migratory insertions of d^6 square-pyramidal complexes. Other complexes are under investigation to probe the generality of these observations.

EXPERIMENTAL SECTION

General Considerations. All manipulations were carried out using standard Schlenk, high-vacuum, and glovebox techniques. Argon was purified by passage through columns of BASF R3-11 (chemalog) and 4 Å molecular sieves. Pentane and methylene chloride were passed through columns of activated alumina and deoxygenated by purging with N_2. Benzene was dried over 4 Å molecular sieves and degassed to remove both oxygen and nitrogen. NMR spectra were recorded on Bruker DRX 400, AMX 300, and 500 MHz instruments and are referenced to residual protio solvent peaks. ^{31}P chemical shifts are referenced to an external H_3PO_4 standard. Since there is a strong ^{31}P−^{31}P coupling in the pincer complexes, many of the ^{1}H and ^{13}C signals exhibit virtual coupling and appear as triplets. These are specified as "vt", with the *apparent* coupling simply noted as *J*. Elemental analyses were carried out by Atlantic Microlab, Inc. (Norcross, GA) or Robertson Microlit Laboratories Inc. (Madison, NJ). All reagents, unless otherwise noted, were purchased from commercial sources and used without further purification. Propylene was used as received from National Specialty Gases (Durham, NC). Ethylene was purchased from Matheson. The syntheses of the phosphinite complexes (POCOP)Ir(H)(Cl) and (POCOP)Rh(H)(Cl) have been previously described in the literature.[14] The abbreviation BAr^f_4 is used to represent the counterion tetrakis(3,5-trifluoromethylphenyl)borate. The ^{1}H and ^{13}C spectral data for BAr^f_4 in CD_2Cl_2 are the same for all complexes listed [^{1}H NMR (CD_2Cl_2) δ 7.72 (s, 8H, H_o), 7.56 (s, 4H, H_p); $^{13}C\{^1H\}$ NMR (CD_2Cl_2) δ 162.2 (q, J_{C-B} = 37.4 Hz, C_{ispo}), 135.2 (C_o), 129.3 (q, J_{C-F} = 31.3 Hz, C_m), 125.0 (q, J_{C-F} = 272.5 Hz, CF_3), 117.9 (C_p)] and are therefore not reported in the characterizations below.

General Procedure for the Synthesis of [(POCOP)M(H)(olefin)][BAr$_4^f$] (6a/b-Ir and 6a/b-Rh). In a Schlenk flask under argon, 1 equiv of (POCOP)M(H)(Cl), 1.1 equiv of $NaBAr^f_4$, and excess olefin were stirred in methylene chloride for 15 min. The reaction mixture was then filtered under an inert atmosphere in a glovebox. The product was isolated after removal of the methylene chloride solvent under reduced pressure.

[(POCOP)Ir(H)(C_2H_4)][BAr^f_4] (***6a-Ir***). The general procedure was employed using (POCOP)Ir(H)(Cl) (0.08 mmol, 50 mg) and $NaBAr^f_4$ (0.089 mmol, 77.9 mg) in CH_2Cl_2 (10 mL) and purging ethylene through the reaction mixture. The color changed from pale red to orange within 5 min, indicating the completion of the reaction. Following filtration and solvent removal, the product was isolated as a pale orange solid (104 mg, 87.7% yield). ^{1}H NMR (500 MHz, CD_2Cl_2): δ 7.22 (t, $^3J_{H-H}$ = 8.0 Hz, 1H, 1-H), 6.92 (d, $^3J_{H-H}$ = 8.0 Hz, 2H, 2-H), 4.15 (s, 4H, C_2H_4), 1.34 (vt, *J* = 7.5 Hz, 18H, P(*t*Bu)$_2$), 1.27 (vt, *J* = 8.0 Hz, 18H, P(*t*Bu)$_2$), −42.83 (b, 1H, Ir*H*). $^{31}P\{^1H\}$ NMR (162 MHz, CD_2Cl_2): δ 182.0. $^{13}C\{^1H\}$ NMR (125.8 MHz, CD_2Cl_2): δ 167.0 (C_q, vt, *J* = 5.6 Hz, 2C, 3-C), 133.8 (C_q, m, 1C, 4-C), 132.3 (CH, s, 1C, 1-C), 107.1 (CH, t, J_{P-C} = 6.0 Hz, 2C, 2-C), 55.1 (CH_2, s, 2C, C_2H_4), 45.7 (C_q, vt, *J* = 12.1 Hz, $C(CH_3)_3$), 42.8 (C_q, vt, *J* = 13.5 Hz, $C(CH_3)_3$), 28.9 (CH_3, vt, *J* = 2.1 Hz, $C(CH_3)_3$), 28.1 (CH_3, vt, *J* = 1.9 Hz, $C(CH_3)_3$). Elemental analysis calculated for $C_{56}H_{56}BF_{24}IrO_2P_2$ (1481.98): C, 45.39; H, 3.81. Found: C, 45.18; H, 3.69.

[(POCOP)Rh(H)(C_2H_4)][BAr^f_4] (***6a-Rh***). The general procedure was employed using (POCOP)Rh(H)(Cl) (0.08 mmol, 43 mg) and $NaBAr^f_4$ (0.089 mmol, 77.9 mg) in CH_2Cl_2 (10 mL) and purging ethylene through the reaction mixture. The color changed from yellow to pale

brown within 15 min, indicating the completion of the reaction. Following filtration and solvent removal, the product was isolated as a brown solid (105 mg, 94.2% yield). ^{1}H NMR (500 MHz, CD_2Cl_2): δ 7.19 (t, $^3J_{H-H}$ = 8 Hz, 1H), 6.85 (d, $^3J_{H-H}$ = 7.5 Hz, 2H), 4.59 (s, 4H, C_2H_4), 1.30 (vt, 18H, P(tBu)$_2$), 1.23 (vt, 18H, P(tBu)$_2$), −28.61 (dt, $^1J_{Rh-H}$ = 50.5 Hz, $^2J_{H-P}$ = 9 Hz, 1H, Rh-*H*). ^{31}P{^{1}H} NMR (162 MHz, CD_2Cl_2): δ 205.26 (d, J_{P-Rh} = 105.3 Hz). ^{13}C{^{1}H} NMR (125.8 MHz, CD_2Cl_2): δ 166.26 (Ar), 130.81 (Ar), 107.01 (Ar), 72.40 (C_2H_4), 43.56 (C(CH$_3$)), 41.52 (C(CH$_3$)), 28.08 (C(CH$_3$)), 27.44 (C(CH$_3$)); one Ar−C resonance not detected. Elemental analysis calculated for $C_{57}H_{58}BF_{24}RhO_2P_2$ (1406.69): C, 48.67; H, 4.16. Found: C, 48.56; H, 3.92.

[(POCOP)Ir(H)(C_3H_6)][BAr$^f_4$] (**6b-Ir**). The general procedure was employed using (POCOP)Ir(H)(Cl) (0.08 mmol, 50 mg) and NaBAr$^f_4$ (0.087 mmol, 77.8 mg) in CH_2Cl_2 (10 mL) and purging propylene through the reaction mixture. The color changed from pale red to orange within 5 min, indicating the completion of the reaction. Following filtration and solvent removal, the product was isolated as a pale orange solid (103 mg, 86% yield). ^{1}H NMR (500 MHz, CD_2Cl_2): δ 7.21 (t, $^3J_{H-H}$ = 8.1 Hz, 1H, 1-H), 6.90 (d, $^3J_{H-H}$ = 7.9 Hz, 1H, 2-H), 6.86 (d, $^3J_{H-H}$ = 8.2 Hz, 1H, 6-H), 6.43 (m, 1H, 8-H), 5.5 (dd, $^3J_{H-H}$ = 12.0 Hz, J_{P-H} = 8.5 Hz, 1H, 7-H$_{trans}$), 3.3 (d, $^3J_{H-H}$ = 8.0 Hz, 1H, 7-H$_{cis}$), 1.9 (d, $^3J_{H-H}$ = 5.5 Hz, 3H, 9-H), 1.46 (d, J_{P-H} = 15.3 Hz, 9H, P(tBu)$_2$), 1.35 (d, J_{P-H} = 14.6 Hz, 9H, P(tBu)$_2$), 1.34 (d, J_{P-H} = 15.3 Hz, 9H, P(tBu)$_2$), 1.17 (d, J_{P-H} = 14.6 Hz, 9H, P(tBu)$_2$), −42.9 (t, J_{P-H} = 11.6 Hz, 1H, Ir*H*). ^{31}P{^{1}H} NMR (162 MHz, CD_2Cl_2): δ 182.7 (dd, J_{P-P} = 260.1 Hz), 175.0 (dd, J_{P-P} = 260.1 Hz). ^{13}C{^{1}H} NMR (125.8 MHz, CD_2Cl_2): δ 167.2 (C$_q$, m, 2C, 3-C and 5-C), 132.4 (CH, s, 1C, 1-C), 131.3 (C$_q$, m, 1C, 4-C), 106.9 (CH, m, 2C, 2-C and 6-C), 77.8 (CH, s, 1C, 7-C), 66.2 (CH$_2$, s, 1C, 8-C), 45.6 (C$_q$, d, J_{P-H} = 22.3 Hz, 2C, C(CH$_3$)$_3$), 42.5 (C$_q$, d, J_{P-H} = 20.5 Hz, 1C, C(CH$_3$)$_3$), 41.9 (C$_q$, d, J_{P-H} = 20.9 Hz, 1C, C(CH$_3$)$_3$), 29.4 (CH$_3$, d, J_{P-H} = 3.5 Hz, C(CH$_3$)$_3$), 29.2 (CH$_3$, d, J_{P-H} = 3.5 Hz, C(CH$_3$)$_3$), 28.4 (CH$_3$, d, J_{P-H} = 2.9 Hz, C(CH$_3$)$_3$), 28.11 (CH$_3$, d, J_{P-H} = 3.5 Hz, C(CH$_3$)$_3$). Elemental analysis calculated for $C_{57}H_{58}BF_{24}IrO_2P_2$ (1496.01): C, 45.76; H, 3.91. Found: C, 45.64; H, 3.84.

[(POCOP)Rh(H)(C_3H_6)][BAr$^f_4$] (**6b-Rh**). The general procedure was employed using (POCOP)Rh(H)(Cl) (0.08 mmol, 43 mg) and NaBAr$^f_4$ (0.087 mmol, 77.8 mg) in CH_2Cl_2 (10 mL) and purging propylene through the reaction mixture. The color changed from pale red to deep red-brown within 5 min. Filtration and solvent removal resulted in regeneration of the starting material, presumably the chloride being scavenged from the solvent. Attempts at isolating **6b-Rh** free of starting material have so far been unsuccessful. Thus, the propylene adduct was characterized *in situ* and in the presence of excess propylene. ^{1}H NMR (500 MHz, CD_2Cl_2): δ 7.17 (t, $^3J_{H-H}$ = 8.0 Hz, 1H, Ar-H), 7.05 (m, 1H, H$_{gem}$), 6.80 (app t, $^3J_{H-H}$ = 8.0 Hz, 1H, Ar-H$_{maj}$), 6.60 (d, $^3J_{H-H}$ = 8.2 Hz, 1H, Ar-*H*$_{min}$), 5.88 (m, 1H, H$_{trans}$), 3.50 (d, $^3J_{H-H}$ = 8.0 Hz, 1H, H$_{cis}$), 1.86 (d, $^3J_{H-H}$ = 5.5 Hz, 3H, Me), 1.48 (d, J_{P-H} = 15.3 Hz, 9H, P(tBu)$_2$), 1.30 (d, J_{P-H} = 14.6 Hz, 18H, P(tBu)$_2$), 1.20 (d, J_{P-H} = 15.3 Hz, 9H, P(tBu)$_2$), −27.28 (dt, 1H, $^1J_{Rh-H}$ = 50.0 Hz, $^2J_{H-P}$ = 8.5 Hz, Rh-*H*$_{min}$), −28.38 (dt, 1H, $^1J_{Rh-H}$ = 50.0 Hz, $^2J_{H-P}$ = 8.5 Hz, Rh-*H*$_{maj}$). ^{31}P{^{1}H} NMR (162 MHz, CD_2Cl_2): δ 203.6$_{maj}$ (dd, J_{Rh-P} = 86.9 Hz, J_{P-P} = 224.5 Hz), 198.8$_{min}$ (dd, J_{Rh-P} = 84.4 Hz, J_{P-P} = 224.6 Hz). ^{13}C{^{1}H} NMR (125.8 MHz, CD_2Cl_2): δ 166.4 (Ar), 132.5 (Ar), 131.2 (Ar), 117.1 (Ar), 107.9 (Ar), 97.5 (br m, C(H)(Me)), 79.8 (br m, CH$_2$), 43.0 (d, J_{P-H} = 21.0 Hz, C(CH$_3$)$_3$), 42.4 (d, J_{P-H} = 21.5 Hz, C(CH$_3$)$_3$), 28.1 (d, J_{P-H} = 3.5 Hz, C(CH$_3$)$_3$), 27.6 (d, J_{P-H} = 3.5 Hz, C(CH$_3$)$_3$), 22.8 (Me$_{prop}$).

Computational Studies. All density functional theory (DFT) calculations were performed by using the Gaussian 03 package.[17] The basis-set/functional selection was based on a prior study of methane binding[18] and consists of the built-in 6-31G** basis set for all non-transition metal atoms, the Stuttgart−Dresden basis set−pseudo relativistic effective core potential combination for the transition metals[19,20] with a single f-type polarization function (exponent = 1.062 (Rh), 0.685 (Ir)) and the functional PBE0, the hybrid variant of PBE that contains 25% Hartree−Fock exchange[21] for geometry optimizations. The PBE0 functional was found to yield results in better agreement with experimental data than the B3LYP[22] functional in an Ir pincer system[23] and has been endorsed as one of the best-performing functionals for late transition metal systems.[24] A similar basis set combined with the PBE0 functional was used to calculate weak Rh···H−C interactions in another system.[25] A comparative set of calculations was carried out with the LAN08(f) basis set−pseudo relativistic effective core potential for the metal,[26] the built-in 6-31G** basis set for all other atoms, and the B3LYP functional. All of the major conclusions of this work hold with either method choice. For each metal−ligand combination, geometries were optimized in the gas phase for the olefin hydride [M(L)(olefin)(H)]$^+$ and the agostic complexes [M(L)(agostic)]$^+$. Frequency calculations were carried out on all minimum structures, and the resulting frequencies all had positive values. The nonscaled vibrational frequencies formed the basis for the calculation of vibrational zero-point corrections and the standard thermodynamic corrections for the conversion of electronic energies to enthalpies and free energies at 298.15 K and 1 atm. The entropy corrections for the highly crowded POCOP−propylene complexes yielded inconsistent results as a function of metal; therefore, the ZPE-corrected electronic energies were used for comparison to experimental data in all cases.

For each M−olefin pair, the transition state for hydride migration and the transition state for in-place rotation were optimized in the gas phase using the synchronous transit-guided quasi-Newton (STQN) method implemented in Gaussian. Frequency calculations yielded one imaginary frequency for all transition states, and IRC calculations were carried out to confirm that the transition state identified connected the correct minima.

Included as Supporting Information are a table of calculated electronic energies, enthalpies, and free energies in the gas phase for all ground states and transition states calculated, as well as tables of Cartesian coordinates (Å) for the optimized structures and transition states in the gas phase.

■ ASSOCIATED CONTENT

Supporting Information. Crystal structure information file for **6b-Ir**, complete calculations for dynamic processes, sample ^{1}H NMR spectra, thorough discussion of variable-temperature NMR behavior, complete ref 17, and full details of calculations including Cartesian coordinates of all optimized geometries. This material is available free of charge via the Internet at http://pubs.acs.org.

■ AUTHOR INFORMATION

Corresponding Author
mbrookhart@unc.edu; schauer@unc.edu

■ ACKNOWLEDGMENT

We gratefully acknowledge the financial support of the NSF (Grant Nos. CHE-0650456 as part of the Center for Enabling New Technologies through Catalysis (CENTC) and CHE-1010170).

■ REFERENCES

(1) See, for example: (a) Hartwig, J. *Organotransition Metal Chemistry: From Bonding to Catalysis*; University Science Books: New York, 2009. (b) Ojima, I.; Eguchi, M.; Tzamarioudaki, M. In *Comprehensive Organometallic Chemistry*; Abel, E. W., Ed.; Pergamon: New York, 1995; p 39.

(2) See, for example: (a) Cross, R. J. In *The Chemistry of the Metal−Carbon Bond*; Hartley, F. R., Patai, S., Eds.; Wiley: New York,

1985; Vol. 2, Chapter 8. (b) Bullock, R. M. In *Transition Metal Hydrides*; Dedieu, A., Ed.; VCH: New York, 1992; p 263.
(3) Brookhart, M.; Green, M. L. H. *J. Organomet. Chem.* **1983**, *250*, 395.
(4) Brookhart, M.; Green, M. L. H.; Wong, L. L. *Prog. Inorg. Chem.* **1988**, *36*, 1.
(5) Brookhart, M.; Green, M. L. H.; Parkin, G. *Proc. Natl. Acad. Sci. U.S.A.* **2007**, *104*, 6908.
(6) Steinke, T.; Shaw, B. K.; Jong, H.; Patrick, B. O.; Fryzuk, M. D.; Green, J. C. *J. Am. Chem. Soc.* **2009**, *131*, 10461–10466.
(7) (a) Green, M. L. H.; Wong, L. L. *J. Chem. Soc., Chem. Commun.* **1988**, 677–679. (b) Derome, A. E.; Green, M. L. H.; Wong, L. L. *New J. Chem.* **1989**, *10*, 747–753. (c) Bercaw, J. E.; Burger, B. J.; Green, M. L. H.; Santarsiero, B. D.; Sella, A.; Trimmer, M.; Wong, L. L. *J. Chem. Soc., Chem. Commun.* **1989**, 734–736. (d) McNally, J. P.; Cooper, N. J. *Organometallics* **1988**, *7*, 1704–1715. (e) Casey, C. P.; Yi, C. S. *Organometallics* **1991**, *10*, 33–35. (f) Tempel, D. J.; Brookhart, M. *Organometallics* **1998**, *17*, 2290–2296.
(8) (a) Xu, R.; Klatt, G.; Wadepohl, H.; Koppel, H. *Inorg. Chem.* **2010**, *49*, 3289–3296. (b) Scherer, W.; Herz, V.; Bruck, A.; Hauf, C.; Reiner, F.; Altmannshofer, S.; Leusser, D.; Stalke, D. *Angew. Chem., Int. Ed.* **2011**, *50*, 1–6. (c) Mitoraj, M. P.; Michalak, A.; Ziegler, T. *Organometallics* **2009**, *28*, 3727–3733 and references therein. (d) Clot, E.; Eisenstein, O. *Struct. Bonding (Berlin)* **2004**, *113*, 1–36.
(9) Brookhart, M.; Lincoln, D. M.; Volpe, A. F., Jr.; Schmidt, G. F. *Organometallics* **1989**, *8*, 1212.
(10) Brookhart, M.; Lincoln, D. M.; Bennett, M. A.; Pelling, S. *J. Am. Chem. Soc.* **1990**, *112*, 2691.
(11) Brookhart, M.; Hauptman, E.; Lincoln, D. M. *J. Am. Chem. Soc.* **1992**, *114*, 10394.
(12) (a) Shiotsuki, M.; White, P. S.; Brookhart, M.; Templeton, J. L. *J. Am. Chem. Soc.* **2007**, *129*, 4058–4067. (b) Tempel, D. J.; Johnson, L. K.; Huff, R. L.; White, P. S.; Brookhart, M. *J. Am. Chem. Soc.* **2000**, *122*, 6686–6700. (c) Killian, C. M.; Johnson, L. K.; Brookhart, M. *Organometallics* **1997**, *16*, 2005–2007. (d) Killian, C. M.; Johnson, L. K.; Brookhart, M. *J. Am. Chem. Soc.* **1999**, *121*, 10634–10635. (e) Rix, F. C.; Brookhart, M. *J. Am. Chem. Soc.* **1995**, *117*, 1137–1138. (f) Johnson, L. K.; Killian, C. M.; Brookhart, M. *J. Am. Chem. Soc.* **1995**, *117*, 6414–6415. (g) Malinoski, J. M.; Brookhart, M. *Organometallics* **2003**, *22*, 5324–5335.
(13) (a) Stromberg, S.; Zetterberg, K.; Siegbahn, P. E. M. *J. Chem. Soc., Dalton Trans.* **1997**, 4147–4152. (b) Musaev, D. G.; Froese, R. D. J.; Morokuma, K. *Organometallics* **1998**, *17*, 1850–1860. (c) Musaev, D. G.; Morokuma, K. *Top. Catal.* **1999**, *7*, 107–123. (d) Michalak, A.; Ziegler, T. *Kinet. Catal.* **2006**, *47*, 310–325. (e) Mitoraj, M.; Michalak, A. *J. Mol. Model.* **2005**, *11*, 341–350. (f) Deubel, D. V.; Ziegler, T. *Organometallics* **2002**, *21*, 1603–1611. (g) Deubel, D. V.; Ziegler, T. *Organometallics* **2002**, *21*, 4432–4441. (h) Michalak, A.; Ziegler, T. *Organometallics* **2003**, *22*, 2660–2669.
(14) (a) M = Ir: Gottker-Schnetmann, I.; White, P. S.; Brookhart, M. *J. Am. Chem. Soc.* **2004**, *126*, 1804–1811. (b) M = Rh: Salem, H.; Shimon, L. J. W.; Leitus, G.; Weiner, L.; Milstein, D. *Organometallics* **2008**, *27*, 2293–2299.
(15) See Supporting Information.
(16) (a) Burdett, J. K. *Inorg. Chem.* **1975**, *14*, 375–382. (b) Cooper, A. C.; Clot, E.; Huffman, J. C.; Streib, W. E.; Maseras, F.; Eisenstein, O.; Caulton, K. G. *J. Am. Chem. Soc.* **1999**, *121*, 97–106. (c) Ujaque, G.; Cooper, A. C.; Maseras, F.; Eisenstein, O.; Caulton, K. G. *J. Am. Chem. Soc.* **1998**, *120*, 361–365.
(17) Frisch, M. J.; , et al. *Gaussian 03*, Revision E.01; Gaussian, Inc.: Wallingford, CT, 2004.
(18) Bernskoetter, W. H.; Schauer, C. K.; Goldberg, K. I.; Brookhart, M. *Science* **2009**, *326*, 553–556.
(19) Andrae, D.; Haeussermann, U.; Dolg, M.; Stoll, H.; Preuss, H. *Theor. Chim. Acta* **1990**, *77*, 123–141.
(20) Martin, J. M. L.; Sundermann, A. *J. Chem. Phys.* **2001**, *114*, 3408–3420.
(21) Perdew, J. P.; Burke, K.; Ernzerhof, M. *Phys. Rev. Lett.* **1996**, *77*, 3865–3868.
(22) (a) Becke, A. D. *J. Chem. Phys.* **1993**, *98*, 5648–5652. (b) Lee, C.; Yang, W.; Parr, R. G. *Phys. Rev. B: Condens. Matter Mater. Phys.* **1988**, *37*, 785.
(23) Ghosh, R.; Zhang, X.; Achord, P.; Emge, T. J.; Krogh-Jesperson, K.; Goldman, A. S. *J. Am. Chem. Soc.* **2007**, *127*, 853–866.
(24) Quintal, M. M.; Karton, A.; Iron, M. A.; Boese, A. D.; Martin, J. M. L. *J. Phys. Chem. A* **2006**, *110*, 709–716.
(25) Montag, M.; Efremenko, I.; Cohen, R.; Leitus, G.; Shimon, L. J. W.; Diskin-Posner, Y.; Ben-David, Y.; Martin, J. M. L.; Milstein, D. *Chem.—Eur. J.* **2008**, *14*, 8183–8194.
(26) Roy, L. E.; Hay, P. J.; Martin, R. L. *J. Chem. Theory Comput.* **2008**, *4*, 1029–1031.